# Path instabilities of air bubbles rising in distilled water

Mingming Wu
*Department of Physics, Occidental College, Los Angeles, CA 90041, USA*

Morteza Gharib
*Graduate Aeronautical Laboratories, California Institute of Technology, Pasadena, CA 91125, USA*
(August 1, 2000)

Experiments are conducted to study the path of a single air bubble (diameter range $0.10-0.20cm$) rising freely in distilled water. The experimental results demonstrate that the bubble shape has a bistable state, *i. e.* the bubble stays in spherical or ellipsoidal shape depending on its generation mechanism. The path of a spherical/ellipsoidal bubble is found to change from a straight path to a zigzag/spiral path via a supercritical/subcritical bifurcation when the Reynolds number of the bubble exceeds a threshold.

PACS numbers: 47.55.Dz, 47.20.-k, 47.27.Vf

The spiral or zigzag motion of air bubbles rising freely in a fluid medium have been observed in various experiments. [1–6] Extensive work has been done to determine the criteria for the onset of path instability. [2–5,7,8] Though appearing to be a simple matter, the path of the bubble itself is observed to be very sensitive to the experimental setup near the instability point, especially to the bubble generation mechanism, the turbulence level in the fluid medium and the contaminations of the fluids. As a consequence, there exists a large range of measured critical Reynolds number, $397 - 670$, above which the path of a single bubble rising in distilled water deviates from a straight line. [2–5] To the authors' knowledge, the exact nature of the path instability is yet to be explored.

The focus of our investigations is on the understanding of the underlying mechanism of the path instability. Recent work by Kelley and Wu [9] on path instabilities of a penny-shaped bubble rising in a Hele-Shaw cell (2-dimensional case) demonstrated that the path of a bubble was changed from a straight path to a zigzag path when the Reynolds number exceeded a critical value. Colored dye visualization experiments showed that such instability was a consequence of vortex shedding in the wake of the bubble, reminiscent of vortex shedding in the wake of a solid cylinder. In the 3-dimensional case where bubbles rise freely in fluids, some intriguing work has been done by Lunde and Perkins [6] where the wake structures of the bubbles rising in tap water were studied using a colored dye visualization technique in the Reynolds number range of 600-1700. The experimental results demonstrated a clear connection between the wake structures and the lateral motions of the bubbles.

In this letter, we present experimental investigations on the path of the rising bubbles in distilled water near and above the path instability point. The main part of the experimental apparatus is the Plexiglas water tank with dimensions of $6'' \times 6'' \times 24''$. At the center of the bottom plate, a specially designed fitting is mounted for the insertion of a hypodermic needle. The bubble is released through the hypodermic needle. One camera is used to take close-up images of the bubble. The camera typically takes an image of $640\times480$ pixels with a viewing window of $1.25cm \times 0.936cm$, in which the lower bound is $\sim 1.5cm$ above the needle tip. The second camera is a specially designed 3-D imaging system, [10] and it is used to map out the (x, y, z) coordinates of the bubble. Here $x$ and $y$ are lateral positions of the bubble, and $z$ is the vertical distance above the needle. The camera obtains $z$ using a quantitative defocusing mechanism [10]. A typical viewing window of the 3-D imaging system is $1.5cm \times 1.5cm \times 20cm$, in which the lower bound is $\sim 20cm$ above the needle tip. It needs to be noted that the camera is designed in such a way that the spatial resolution in the x-y plane is about 15 times better than the resolution along the z direction, making it an ideal instrument for recording trajectories with small lateral movements. Extreme caution was taken to keep the tank as clean as possible. Doubly deionized and doubly distilled water was used. Large bubbles were driven through the tank for removing the surface-active contaminants prior to each experimental run. The temperature of the water tank was $T = 21.5 \pm 0.3^o$C during the experimental runs except for those explicitly indicated. The surface tension of the water is measured to be 71.6dyn/cm using a Fisher Scientific tensiometer (Tensiomat Model 21). The kinetic viscosity $\nu = 0.00968$ cm$^2$/s is given by Ref. [11].

Two different bubble generation methods have been used. The first one is to attach the hypodermic needle directly to a syringe filled with air. The syringe is pushed gently until a bubble is formed at the tip of the needle and then is pinched off from the needle. The size of the bubble depends on the inner diameter of the needle and the shape of the needle tip. Using this pinch-off method, bubbles with an ellipsoidal shape have been generated consistently. The aspect ratios (long axis versus short axis ) of the bubbles are between 1.12-1.89 for bubbles of diameter range of $0.10cm - 0.20cm$. The bubble di-

ameter $d$ here is defined as $(6V/\pi)^{1/3}$, where $V$ is the volume of the bubble. $V$ is obtained using the close-up image taken by the CCD camera. Fig. 2a shows a typical image of an ellipsoidal bubble. For the second bubble generation method, the hypodermic needle is attached to a three-way valve, of which one way is connected to a syringe filled with water and the other to a syringe pump filled with air. The hypodermic needle has a specially designed capillary tube with a flat top. The inner diameter of the tube is $0.121cm$ and the length of the tube is $3''$. To generate a bubble, a desired volume of air is pushed into the lower end of the capillary tube by the syringe pump, and then the direction of a three-way valve is switched so that the bubble can be gently pushed out of the capillary tube by the syringe filled with water. Using this gentle-push method, bubbles of a nearly spherical shape are generated consistently. The aspect ratios are between $1.00 - 1.07$ for bubbles in the diameter range of $0.10 - 0.20cm$. A typical spherical bubble image is shown in Fig. 2b

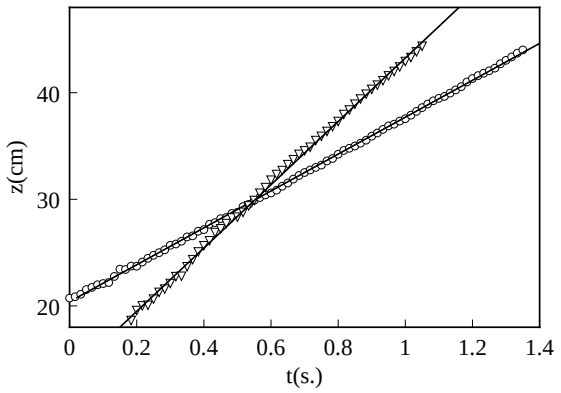


FIG. 1. Vertical displacement $z$ of the rising bubble versus time $t$. ◯: data for nearly spherical bubble of $d = 0.195cm$ and vertical velocity of $17.3cm/s$. ▽: data for ellipsoidal bubble of $d = 0.199cm$ and vertical velocity of $29.8cm/s$.

Preliminary studies are done on the shapes of the bubbles as they detach from the top of the needle using a high speed video camera (1000 frame/s). It is found that the bubbles undergo two different sequences of transient shapes under two different generation mechanisms. In the case of the pinch-off method, a thin neck is formed at the rear of the bubble at the point of detachment. This thin neck gives rise to a strong axial jet around the bubble surface and the jet travels upward and downward along the vertical axis alternatively. The jet dampens as the bubble reaches its final ellipsoidal shape. During the transient period, the bubble travels vertically upward, and gain a relatively large velocity compared to the case of the gentle-push method. Similar phenomena were observed by Longuet-Higgins *et al* [13]. In the case of the gentle-push method, no jet is present due to the lack of curvature singularity at the point of detachment. The bubble usually travels side ways, and undergoes a sequence of shape changes that varies from case to case. In both situations, the shape of the bubble reaches its steady state when it rises $\sim 2cm$ above the needle, and stays in the same shape (spherical or ellipsoidal shape) as it travels vertically to finish its journey of $\sim 60cm$.

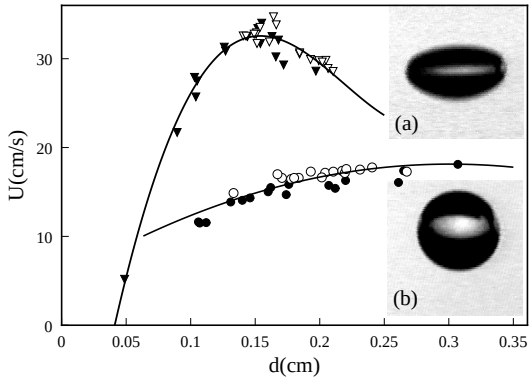


FIG. 2. Terminal velocity $U$ versus diameter $d$ of ellipsoidal bubbles (upper curves) and nearly spherical bubbles (lower curves). Inset (a) is an image of an ellipsoidal bubble with $d = 0.172cm$, inset (b) is an image of a nearly spherical bubble with $d = 0.174cm$. Solid lines are guidelines. Solid symbols are data taken at $T = 24.5^{o}C$

For a typical experimental run, a series of 60 images is recorded at a rate of 30 images per second using the 3-D camera. Each image contains information necessary for inferring the (x,y,z) coordinates of the bubble. The trajectories of the bubbles are then extracted from the image series. The vertical displacement $z$ of the bubble versus time $t$ is shown by Fig. 1. The vertical velocities $U$ of the bubbles are obtained from the linear fits to $z$ versus $t$ data. Fig. 1 shows that the vertical velocities are essentially constant in the $z$ range of measurement. Further, we plotted the velocity versus diameter $d$ of the bubble (See Fig. 2). It is shown that the ellipsoidal bubbles move much faster than the spherical bubbles in the diameter range of $0.1 - 0.2cm$.

For nearly spherical bubbles, the straight path of the bubble is changed to a zigzag path as $Re$ exceeds a critical value $Rec$. Here, $Re$ is defined as $Ud/\nu$. Typical planar zigzag path of the bubble is shown in Fig. 3a. A zigzag function is used to fit the zigzag path, and the amplitude $A$ and the frequency $f$ of the zigzag path is obtained from the fitted parameters. In Fig. 4a, the dimensionless amplitude squared of the zigzag path is plotted as a function of Reynolds number. As seen, the amplitude squared is linearly related to the Reynolds number near the onset of the path instability, a signature of supercritical bifurcation. The linear extrapolation of the line gives the critical Reynolds number of $Rec = 280 \pm 20$. The Strouhal number $fd/U$ is in the range of $0.08 - 0.12$ for Reynold number range of $200 - 600$.

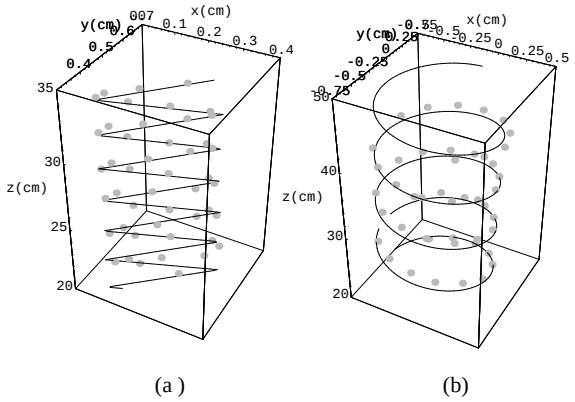


FIG. 3. (a) Zigzag path of a nearly spherical bubble at $Re = 362$. Solid line is a fit to a zigzag function. (b) Spiral path of an ellipsoidal bubble at $Re = 613$. Solid line is a fit to a spiral function. In both (a) and (b), the dotted lines are from experiments.

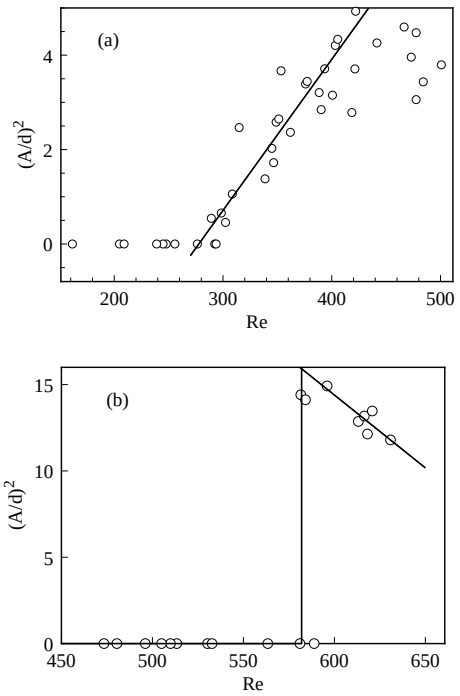


FIG. 4. Curves of dimensionless amplitude squared versus $Re$ for (a) nearly spherical bubbles and (b) ellipsoidal bubbles. Dotted lines are from experiments. Solid line in (a) is a fit to a linear function and in (b) is a guideline.

For ellipsoidal bubbles, the straight path of the bubble is changed to a spiral path as shown in Fig. 3b when the Reynolds number exceeds a critical value. The measured spiral path is fitted to a spiral function, where the amplitude $A$ and frequency $f$ of the spiral path are obtained from the fitted parameters. The curve of dimensionless amplitude squared versus Reynolds number Fig. 4b shows that the spiral path instability occurs at $Rec = 582 \pm 20$ via a subcritical bifurcation. The Strouhal number at the onset is $\sim 0.02$. The percent error of $A/d$ is estimated to be $\sim 7\%$ and $Re \sim 8\%$

It is known that the bubble dynamics is very sensitive to the contaminations in water. However, the reference for clean water among current literatures is not yet determined. We believe that using the surface tension value is the best known criterion for measuring the cleanness of the water. We measured our water's surface tension to be 71.6dyn/cm at a temperature of $21.5^o$(CRC reports 72.52dyn/cm), which is very close to that reported recently by Maxworthy et al [14] (71.68dyn/cm at $20^o$, whereas CRC reports 72.75 dyn/cm for the same temperature) using clean water. We also compared our drag coefficient curves with those from recent experiments by Duineveld [5] using hyper-clean water. The drag coefficient $C_d$ is defined as $4gd/3U^2$, $g$ is the gravitational constant. A relatively good agreement between our data and that of Duineveld for the ellipsoidal bubbles can be seen within the experimental uncertainty. Note that Duineveld used the pinch-off method in his experiment. Our data also agrees well with the analytical results of Moore [12] where shape changes are taken into consideration. For the nearly spherical bubbles, the drag coefficients are unusually large, they are, in fact, greater than those of solid spheres [16]. Further work is in progress to study this new phenomena. Fig. 5 also shows slight temperature dependency of the drag coefficient in the case of spherical bubbles.

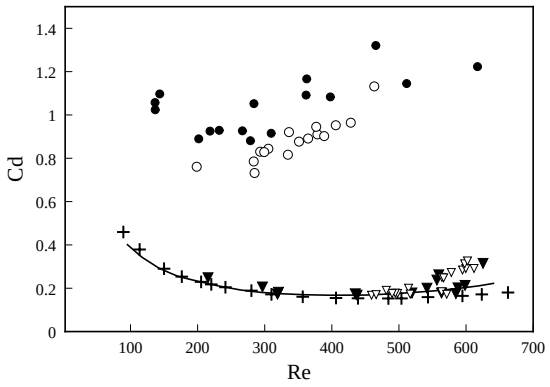


FIG. 5. Drag coefficient $C_d$ vs. Reynolds number $Re$. Data taken at $T = 24.5^oC$ (open triangles) and $21.5^oC$ (solid triangles) for ellipsoidal bubbles; +: data of Duineveld at $T = 19.6^oC$ for ellipsoidal bubbles[5]; • and ∘: data taken at $T = 24.5^oC$ and $21.5^oC$ for nearly spherical bubbles; the solid line is from analytical result of Moore[12].

The above experimental results demonstrate that the underlying mechanisms for path instabilities of spherical and ellipsoidal bubbles are very different. For the case of spherical bubbles, a colored dye visualization experiment was carried out. The results were consistent with those of Lunde and Perkins [6], where hairpin vortices were ob-

served to shed periodically from the alternate rear sides of the zigzag bubble. This suggests that the zigzag path instability is caused by the vortex shedding in the wake of the bubble, in a similar way as in the 2-D situation. [9] However, the sources of the vorticity in the wake of the spherical bubbles are yet to be determined. From the unusually large drag coefficient (Fig. 5), we conjecture that the vorticities may come from both the slight deformation of the bubble and the curvature of the bubble. For the case of ellipsoidal bubbles, the colored dye visualization experiments by Lunde and Perkins [6] revealed two continuous vortex filaments at the rear of the bubbles. It needs to be mentioned that the colored dye itself introduces contaminations to the water, thus a direct comparison with the above experimental results are not possible. The exact cause for the spiral instability is yet to be explored. From the high-speed images, it is noticed that the short axis of the ellipsoidal bubble is always aligned with the direction of the bubble motion, similar to the observation of Miyagi, [17] it is likely that the ellipsoidal bubble spins around its short axis as it spirals up.

In summary, we found that the shape of the air bubbles has a bistable state within the diameter range of $0.1 - 0.2cm$. It can either be in spherical or ellipsoidal shape depending on its generation mechanisms. The spherical bubbles undergo a zigzag path instability via a supercritical bifurcation, and the ellipsoidal bubbles undergo a spiral path instability via a subcritical bifurcation as the Reynolds number exceeds a threshold.

Wu would like to thank Professor Maxworthy for an insightful discussion on the subject. Wu would also like to thank members of Gharib's group who offered generous help during her summer stay at Caltech. This work is supported by the Office of Naval Research (N00014-98-1-0017), the Petroleum Research Fund (ACS-PRF# 32904-GB9) and the Research Corporation (CC4612).

[1] P. G. Saffman, J. Fluid Mech. **1**, 249 (1956).
[2] R. A. Hartunian and W. R. Sears, J. Fluid Mech. **3**, 27 (1957).
[3] N. M. Aybers and A. Tapucu, Warme- und Stoffubertragung Bd. 2, 118(1969).
[4] H. Tsuge and S. Hibino, J. Chem. Engng. Japan **10**, 66 (1977).
[5] P. C. Duineveld, J. Fluid Mech. **292**, 325(1995).
[6] K. Lunde and R. J. Perkins, Paper no. FEDSM97-3530, ASME-FED Summer Meeting, Vancouver, Canada , 1997.
[7] G. Ryskin, L. G. Leal, J. Fluid Mech. **148**, 19 (1984).
[8] D. I. Meiron, J. Fluid Mech. **198**, 101 (1989).
[9] Erin Kelley and Mingming Wu, Phys. Rev. Letts. **29**, 1265 (1997).
[10] C. E. Willert and M. Gharib, Experiments in Fluids **12**, 353 (1992).
[11] R. C. Weast, *CRC handbook of chemistry and physics,* 64th ed. (CRC press, West Palm Beach, Florida, 1985).
[12] D. W. Moore, J. Fluid Mech. **23**, 749(1965).
[13] Michael S. Longuet - Higgins, Bryan R. Kerman and Kund Lunde, J. Fluid Mech. **230**, 365(1991).
[14] T. Maxworthy, C. Gnann, M. Kürten and F. Durst, J. Fluid Mech. **321**, 421 (1996).
[15] T. Maxworthy, Private communication, 1998.
[16] R. Clift, J. R. Grace and M. E. Weber, *Bubbles, Drops and Particles*, pg. 111, (Academic, 1978).
[17] O. Miyagi, Technol. Rep. Tohoku Univ. **5**, 135(1925).